Supplemental Information for: *Implications of Reduced-Complexity Aerosol Thermodynamics on Organic Aerosol Mass Concentration and Composition over North America*

Camilo Serrano Damha[1], Kyle Gorkowski[2], and Andreas Zuend[1]

[1]Department of Atmospheric and Oceanic Sciences, McGill University, Montreal, Quebec, Canada
[2]Earth and Environmental Sciences Division, Los Alamos National Laboratory, Los Alamos, New Mexico, USA

Correspondence: Camilo Serrano Damha (camilo.serranodamha@mail.mcgill.ca) and Andreas Zuend (andreas.zuend@mcgill.ca)

Table of Contents

S1 Implementation of the BAT-VBS model in GEOS-Chem

Our implementation of the BAT-VBS model in GEOS-Chem involved two main steps. First, the molecular properties of organic surrogate species required by the BAT-VBS model had to be estimated. Second, the equations of the dry OA partitioning scheme of GEOS-Chem were replaced by the BAT-VBS model.

The approximate molar masses (M_j) and oxygen-to-carbon ratios (O:C$_j$) of organic compounds needed for our updated BAT-VBS scheme in the GEOS-Chem model were estimated using the molecular corridors approach of Shiraiwa et al. (2014). The molecular corridors allow us to relate pure-component saturation mass concentrations of organics (C_j°) to O:C$_j$. The slopes of the two-dimensional space of M_j vs. $\log_{10} C_j^\circ$ are indicative of the typical increase in molar mass associated with a decrease in volatility. The molar mass vs. volatility slopes limiting the two-dimensional space set the range of O:C$_j$ values expected based on 909 oxidation products considered by Shiraiwa et al. (2014). Among the different compound classes considered, *n*-alkanes have the lowest polarity with an O:C$_j$ of 0, while sugar alcohols are the most polar compounds with an O:C$_j$ of 1. This oxygen content range is used in our work to estimate the O:C of OA species in GEOS-Chem, even though organic compounds with higher O:C can be found in aerosol samples. In order to make a direct comparison between the BAT-VBS model and the default VBS approach of GEOS-Chem in terms of OA organic mass concentration predictions, we opted to use the same VBS as described in Pye et al. (2010). To use the information given by molecular corridors, C_j° values are assumed to be equal to the (dry-state) effective saturation mass concentrations ($C_j^\circ \approx C_j^*$); the latter are provided by the default OA scheme of the GEOS-Chem model. The default GEOS-Chem model assigns a M_j of $150.0\ \mathrm{g\,mol^{-1}}$ to every TSOA and ASOA species, which seems unrealistic, especially for oxygenated low-volatility organic compounds (LVOCs) and extremely low-volatility organic compounds (ELVOCs). Likewise, a M_j of $12.0\ \mathrm{g\,mol^{-1}}$ is (incorrectly) assigned to every POA and OPOA species. Those M_j values are irrelevant for solving the equilibrium OA organic mass concentration in the default OA scheme. However, the default values of M_j needed to be corrected for use by the BAT-VBS model in GEOS-Chem, as they are required in the calculation of C_j^* (Eq. (1)). The first step to determine the M_j values of organic compounds (volatility bins) within each of the five precursor types is based on approximating the M_j vs. $\log_{10} C_j^\circ$ slope of each OA precursor. This can be done by estimating the limiting M_j values (i.e., M_j of the most volatile organic compound and M_j of the least volatile organic compound) of each type of OA precursor. The M_j values of the remaining species can then be calculated using the linear equation corresponding to the OA precursor type. For example, in the case of the TSOA compound class, an equation for the linear relationship between M_j and $\log_{10} C_j^\circ$ can be obtained based on the properties of TSOA0 and TSOA3 (Table 2). Since the $\log_{10} C_j^\circ$ values are provided by the 1D VBS of the GEOS-Chem model, we can then calculate the corresponding M_j values of TSOA1 and TSOA2 using the linear equation of the TSOA compound class. The O:C$_j$ ratios of TSOA0, TSOA1, TSOA2, and TSOA3 can then be approximated using the molecular corridor relationship for every pair of $\log_{10} C_j^\circ$ and M_j values, assuming that O:C$_j$ increases from 0 to 1 between the limits of the red envelope at fixed $\log_{10} C_j^\circ$ in Fig. S1. In the particular case of POA and OPOA, the molecular corridor is instead used to estimate M_j values from every pair of $\log_{10} C_j^\circ$ and O:C$_j$ values given that the GEOS-Chem model provides the global mean organic-mass-to-organic-carbon ratios of POA

and OPOA (1.4 and 2.1 for POA and OPOA, respectively), which can be related to O:C$_j$ as follows:

$$\mathrm{O:C}_j = \left(\frac{12}{15}\right)(\mathrm{OM:OC}_j) - \frac{14}{15}, \tag{S1}$$

where OM:OC$_j$ is the organic-mass-to-organic-carbon ratio of species j.

The BAT model assigns one representative functional group to each organic component to represent its water affinity. Of all the options available in terms of functional group, we found that using the BAT model with the ketone effective functional group produces consistent hydrophilic/hydrophobic behavior with the more robust Aerosol Inorganic–Organic Mixtures Functional groups Activity Coefficients (AIOMFAC) thermodynamic model (Zuend et al., 2008, 2011). As such, we decided to set ketone as the average functionality that characterizes each organic component.

A schematic of all the OA species considered in GEOS-Chem is shown in Fig. S2. The properties of these species are summarized in Table 2.

Gas-phase reactions take place between oxidants (e.g., O_3 or OH,NO, HO_2, NO_3 radicals) and OA precursors (e.g., terpenes, isoprene, light aromatics, intermediate-volatility organic compounds, primary semivolatile organic compounds, and oxidized semivolatile organic compounds) in each grid cell and time step of the GEOS-Chem model. The organic oxidation products distribute their mass between the gas phase and the aerosol phase. To achieve equilibrium and estimate the aerosol mass fraction (AMF) of each oxidation product, the default OA scheme of the GEOS-Chem model solves an implicit equation for the total OA organic mass concentration, which only contains dry organic mass (i.e., without considering the OA water uptake). In our simulations, the GEOS-Chem model considers primary and secondary OA species as semivolatile. The equation to solve, derived from absorptive gas–particle partitioning theory (i.e., vapor–liquid equilibrium) (Pankow, 1994, 2003; Donahue et al., 2006; Zuend et al., 2010) and mass balance on each oxidation product, is:

$$\frac{\sum_j \left(C_j^{\mathrm{gas}} + C_j^{\mathrm{SV\,OA}}\right)}{C_j^* \left(1 + \frac{C_{org}^{\mathrm{OA}}}{C_j^*}\right)} = 1, \tag{S2}$$

where $C_j^{\mathrm{SV\,OA}}$ is the OA organic mass concentration, C_j^{g} is the gas-phase organic mass concentration, and C_j^* is the gas–particle partitioning coefficient, also known as the effective saturation mass concentration, of each semivolatile species j. $C_{org}^{\mathrm{OA}} = \sum_j C_j^{\mathrm{SV\,OA}}$ is the total OA organic mass concentration. The VBS solver determines C_{org}^{OA} implicitly from Eq. (S2) by varying its value until convergence is achieved.

The implicit equation for $C_{org}^{\mathrm{SV\,OA}}$ (Eq. (S2)) has a solution only when (Chung and Seinfeld, 2002):

$$\sum_j \frac{C_j^{\mathrm{SV\,OA}} + C_j^{\mathrm{gas}}}{C_j^*} > 1, \tag{S3}$$

where C_j^{g} is the gas-phase mass concentration of each organic component j. Once C_{org}^{OA} is calculated implicitly from Eq. (S2), the aerosol mass fraction (AMF) of each organic component j can be determined, assuming constant, RH-independent C_j^* values, from:

$$\xi_j = \left(1 + \frac{C_j^*}{C_{org}^{\mathrm{OA}}}\right)^{-1}, \tag{S4}$$

where ξ_j is the AMF of each organic species j. In turn, the OA organic mass concentration of each organic species j is then determined by:

$$C_j^{\mathrm{SV\,OA}} = \xi_j \times C_j^{\mathrm{gas+SV\,OA}}, \tag{S5}$$

where $C_j^{\mathrm{gas+SV\,OA}}$ is the total (gas-phase plus particle-phase) mass concentration of organic species j.

The implementation of the BAT-VBS model into GEOS-Chem increases the number of independent variables since C_j^* values are no longer constant for a given T. They are then also a function of OA water content (or, indirectly, RH). Water uptake alters the particle-phase mole fractions and mole-fraction-based activity coefficients of organic species j, in addition to the mass-concentration-weighted harmonic mean molar mass of OA (Serrano Damha et al., 2024). As a result, the procedure described through Eqs. (S2)–(S4) needs to be modified as convergence cannot be achieved only by iterating over C_{org}^{OA} since C_j^* cannot be considered constant. Instead, the BAT-VBS model solves a system of coupled algebraic equations numerically by iterating over ξ_j (Gorkowski et al., 2019). This means that updated values for C_{org+w}^{OA} (Eq. (2)) and C_j^* (Eq. (1)) are calculated during every VBS solver iteration step until ξ_j converges, slightly increasing the computational cost of a nonideal VBS approach in comparison to the standard (dry) VBS of GEOS-Chem.

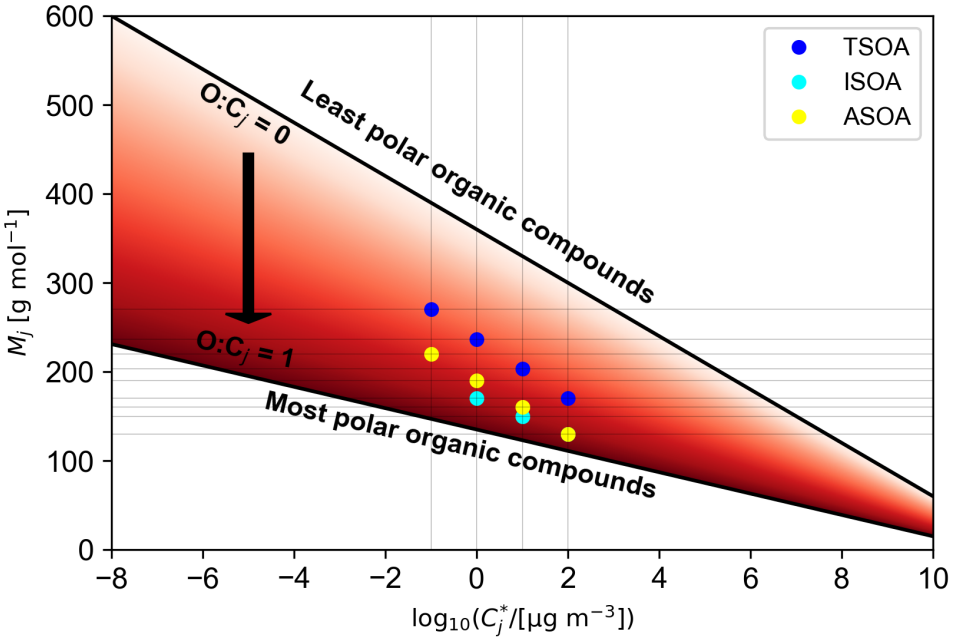

Figure S1. Molecular corridors describing the relationship between molar masses, effective saturation mass concentrations at 298 K, and elemental oxygen-to-carbon ratios of OA organic species (adapted from Fig. 4 of Shiraiwa et al. (2014)). The O:C$_j$ ratios of TSOA, ASOA, and ISOA species were estimated using the molar mass vs. volatility space depicted by the red envelope. The least polar organic compounds (O:C$_j$ = 0) reside in the upper limit of the envelope. The most polar organic compounds (O:C$_j$ = 1) reside in the lower limit of the envelope.

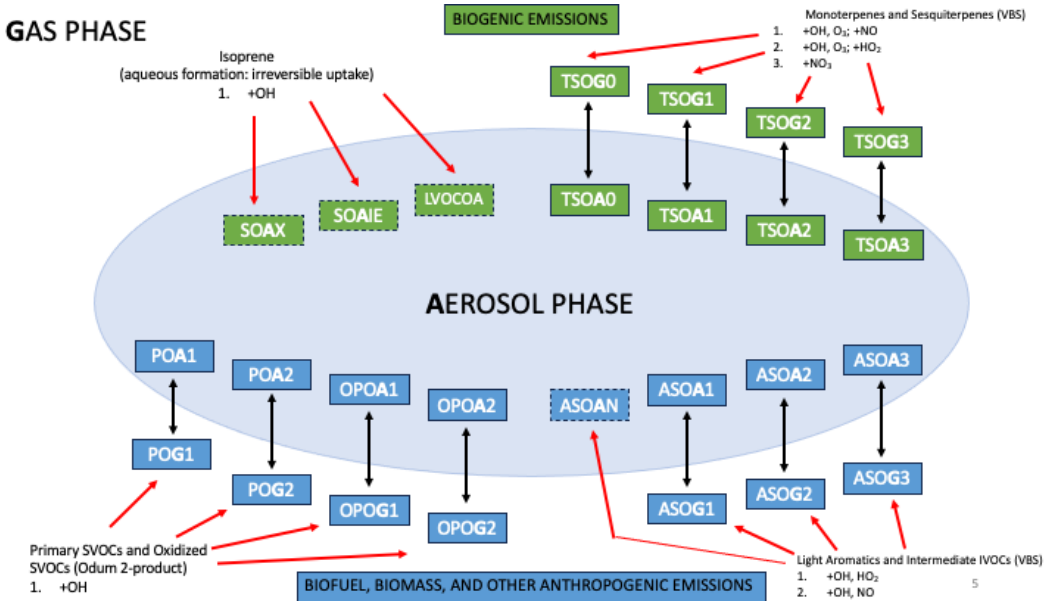

Figure S2. Schematic of all the OA species considered in the GEOS-Chem model (adapted from Fig. 1 in Pye et al. (2010)). OA species are in boxes. Dashed boxes and unidirectional red arrows across the aerosol/gas interface indicate OA species that do not partition to the gas phase. Solid boxes and bidirectional black arrows across the aerosol/gas interface indicate OA species that can partition between the gas phase and the particle phase. Green boxes represent OA species from biogenic sources. Blue boxes represent OA species from anthropogenic sources. As described in Pye et al. (2010), the gas–particle partitioning is parameterized with either a unique 1D VBS with four C_j^* bins, in the case of TSOA and ASOA, or an Odum 2-product fit with two C_j^* bins, in the case of POA and OPOA. Isoprene-derived OA is modeled using an aqueous phase irreversible reactive uptake scheme by Marais et al. (2016). The OA species from terpenes are TSOA0 ($C_j^* = 0.1\ \mu g\,m^{-3}$), TSOA1 ($C_j^* = 1\ \mu g\,m^{-3}$), TSOA2 ($C_j^* = 10\ \mu g\,m^{-3}$), and TSOA3 ($C_j^* = 100\ \mu g\,m^{-3}$). The OA species from isoprene are SOAGX ($C_j^* = 0\ \mu g\,m^{-3}$), SOAIE ($C_j^* = 0\ \mu g\,m^{-3}$), and LVOCOA ($C_j^* = 0\ \mu g\,m^{-3}$). The OA species from light aromatics & intermediate-volatility organic compounds are ASOAN ($C_j^* = 0\ \mu g\,m^{-3}$), ASOA1 ($C_j^* = 1\ \mu g\,m^{-3}$), ASOA2 ($C_j^* = 10\ \mu g\,m^{-3}$), and ASOA3 ($C_j^* = 100\ \mu g\,m^{-3}$). The OA species from primary semivolatile organic compounds are POA1 ($C_j^* = 1646\ \mu g\,m^{-3}$) and POA2 ($C_j^* = 20\ \mu g\,m^{-3}$). the OA species from oxidized semivolatile organic compounds are OPOA1 ($C_j^* = 16.46\ \mu g\,m^{-3}$) and OPOA2 ($C_j^* = 0.2\ \mu g\,m^{-3}$). The reference T for C_j^* of TSOA and ASOA species is 298 K. The reference T for C_j^* of POA and OPOA species is 300 K.

S2 Comparison between Water-Sensitive and Dry OA Schemes at Dry Conditions

The water-sensitive (introduced) and dry (default of GEOS-Chem) OA partitioning schemes were compared at dry conditions (RH = 0 %) by running the GEOS-Chem model over North America for July and January 2019. The absolute and relative differences in mean OA organic mass concentrations over the North American subdomain, averaged over the 72 vertical levels and 248 time steps (3-hourly data for 31 days), are shown in Fig. S3. The absolute and relative differences in mean OA organic mass concentrations over the North American subdomain, averaged over the 248 time steps (3-hourly data for 31 days), are shown in Fig. S4. The dry (default) OA scheme is used as the reference to calculate the differences between OA partitioning schemes. The absolute differences in mean OA organic mass concentrations between the two OA partitioning schemes at dry conditions (RH = 0 %) are negligible. The highest relative differences in mean OA organic mass concentrations between the two OA partitioning schemes at dry conditions (RH = 0 %) are encountered in grid cells where the OA organic mass concentrations are extremely low (e.g., over the ocean). This result serves as a validation point for our implementation, as the water-sensitive OA scheme at dry conditions should predict the same OA organic mass concentration as the dry (default) OA scheme. The absolute and relative differences in OA organic mass concentration are attributed to the different OA partitioning solvers and tolerances used by the two OA partitioning schemes. To estimate more accurately the enhancement of OA organic mass concentration induced by the water-sensitive OA partitioning scheme, we decided to use the BAT-VBS model at dry conditions (RH = 0 %) as the OA partitioning scheme of reference in our results.

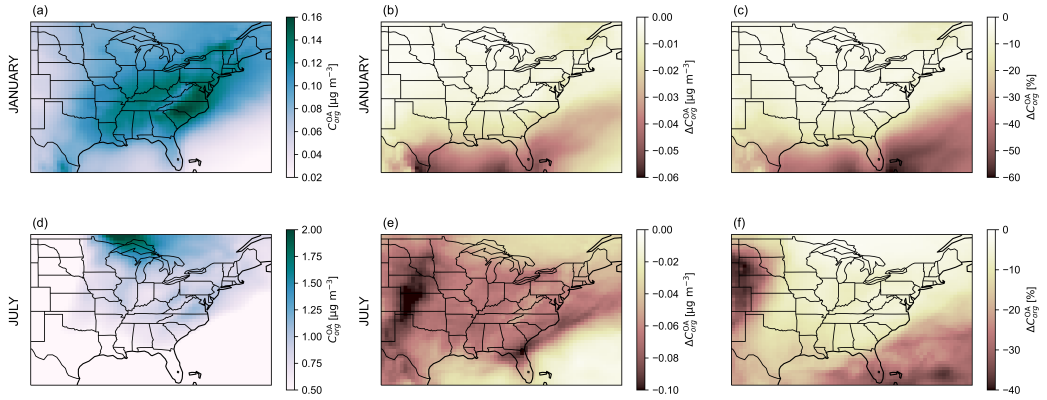

Figure S3. Comparison between the dry (default of GEOS-Chem) and water-sensitive (BAT-VBS model) OA schemes in terms of predicted mean OA organic mass concentration at dry conditions (RH = 0 %) for January and July 2019. The mean is calculated over the 72 vertical levels (0.058 km to 78.146 km) and 248 time steps (3-hourly data for 31 days) of the GEOS-Chem nested simulation. Panels **(a)** and **(d)** show the mean OA organic mass concentration predicted by the introduced water-sensitive OA scheme (BAT-VBS model) at RH = 0 %. Panels **(b)** and **(e)** show the (small) absolute difference in mean OA organic mass concentrations. Panels **(c)** and **(f)** show the relative difference in mean OA organic mass concentrations. The absolute and relative differences are calculated using the default (dry) OA scheme of GEOS-Chem as the reference ($C^{\mathrm{OA}}_{org,\mathrm{BAT-VBS}}$ (RH = 0 %)) - $C^{\mathrm{OA}}_{org,\mathrm{dry}}$).

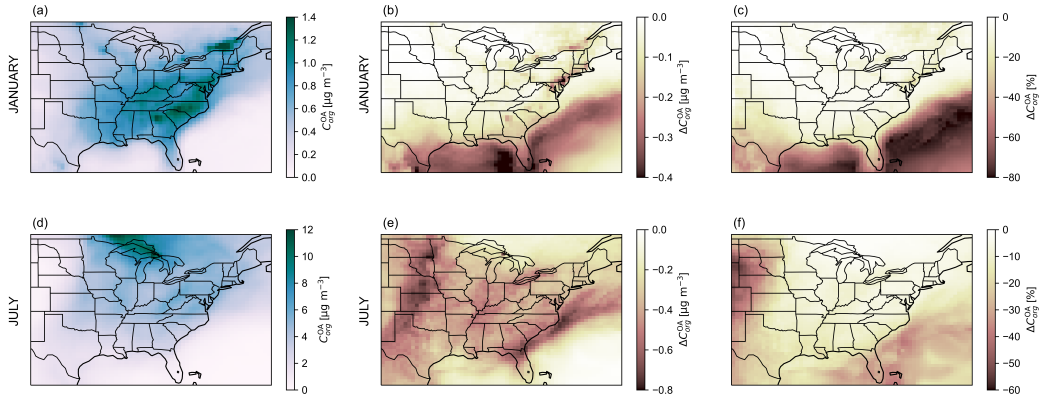

Figure S4. Comparison between the dry (default of GEOS-Chem) and water-sensitive (BAT-VBS model) OA schemes in terms of predicted mean surface OA organic mass concentration at dry conditions (RH = 0 %) for January and July 2019. The mean is calculated over the 248 time steps (3-hourly data for 31 days) of the GEOS-Chem nested simulation. The surface level is the lowest atmospheric level of the GEOS-Chem model. Panels **(a)** and **(d)** show the mean OA organic mass concentration predicted by the introduced water-sensitive OA scheme (BAT-VBS model) at RH = 0 %. Panels **(b)** and **(e)** show the (small) absolute difference in mean OA organic mass concentrations. Panels **(c)** and **(f)** show the relative difference in mean OA organic mass concentrations. The absolute and relative differences are calculated using the default (dry) OA scheme of GEOS-Chem as the reference ($C_{org,\mathrm{BAT-VBS}}^{\mathrm{OA}}$ (RH = 0 %)) - $C_{org,\mathrm{dry}}^{\mathrm{OA}}$).

S3 Mass Fractions of OA Compound Classes

The contribution of organic compounds from biogenic and anthropogenic sources to the OA is expressed as their mass fractions with respect to the OA organic mass concentration (f_{org}). The monthly mean mass fractions of organic species from biogenic and anthropogenic sources at the first atmospheric level ($0.058\ \mathrm{km}$) of GEOS-Chem is shown in Fig. S5 for January and July 2019. Organic species from biogenic sources include the terpenes (TSOA) and isoprene (ISOA) compound classes. Organic species from anthropogenic sources include light aromatics and intermediate-volatility organic compounds (ASOA), primary semivolatile organic compounds (POA), and oxidized semivolatile organic compounds (OPOA). Their contributions to the monthly mean OA organic mass concentration at the first atmospheric layer are shown in Fig. S6.

The water-sensitive (updated) OA scheme that was used in GEOS-Chem in this work captures the variation of the effective volatility of organic species (C_j^*) with RH, a feature that the dry (default) OA scheme is missing. At RH > $0\ \%$ conditions, the water-sensitive OA scheme predicts lower C_j^* values than at dry conditions, and thus more OA organic mass concentration than the dry OA scheme (Fig. 1c, f). The individual contributions of organic compounds to the enhancement of OA organic mass concentration (when using the water-sensitive scheme instead of the dry scheme) are expressed as the ratio of their individual absolute difference in OA organic mass concentration and the cumulative absolute difference in OA organic mass concentration ($f_{\Delta org}$) considering all compound classes. The monthly mean individual contributions of the TSOA, ISOA, ASOA, POA, and OPOA compound classes to the monthly mean cumulative OA organic mass concentration enhancement at the first atmospheric layer ($0.058\ \mathrm{km}$) are shown in Figs. S7–S11 for January and July 2019.

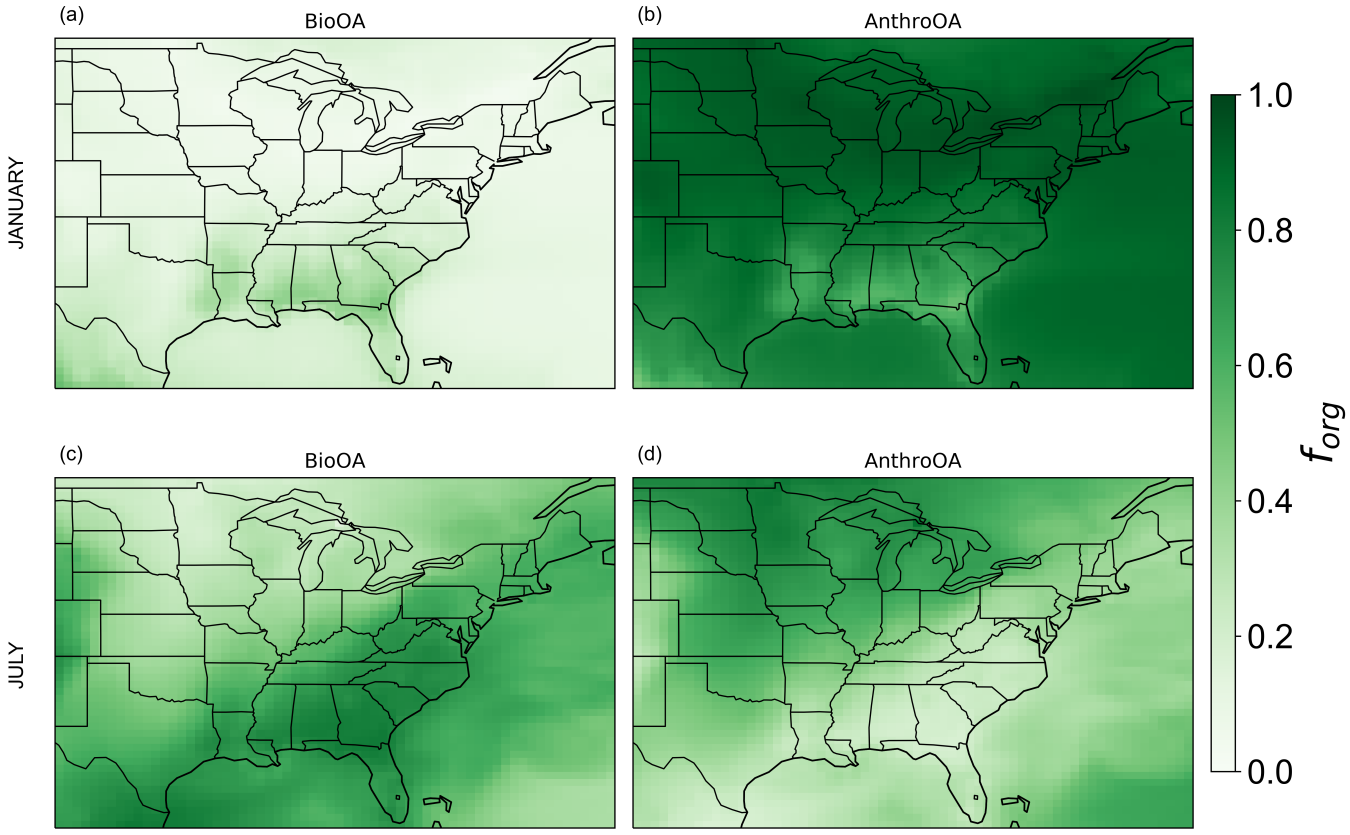

Figure S5. January 2019 (top panels) and July 2019 (bottom panels) monthly mean surface contribution of biogenic and anthropogenic OA species to the OA organic mass concentration, expressed as the organic mass fraction f_{org}. Panels **(a)** and **(c)** show the contribution from biogenic sources (BioOA). Panels **(b)** and **(d)** show the contribution from anthropogenic sources (AnthroOA).

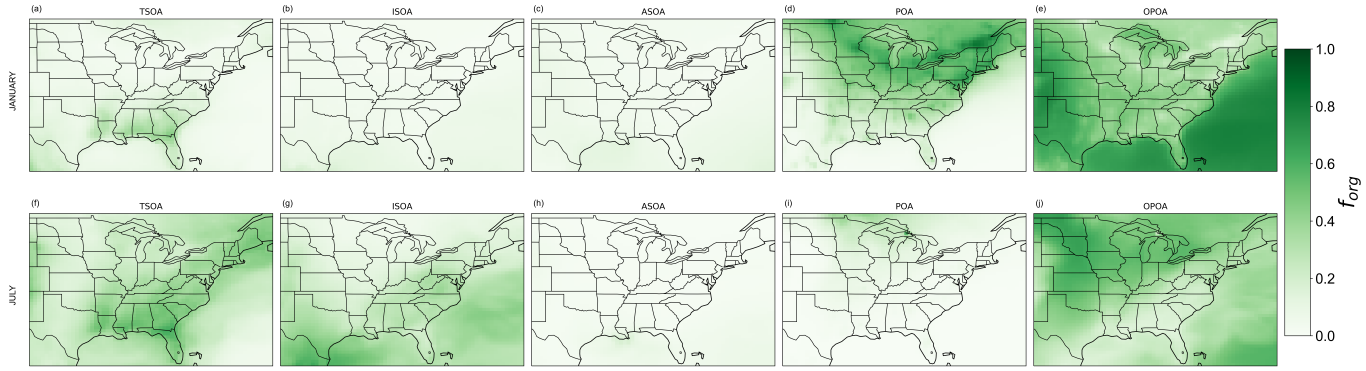

Figure S6. January 2019 (top panels) and July 2019 (bottom panels) monthly mean surface contribution of OA compound classes to the OA organic mass concentration, expressed as the organic mass fraction f_{org}. Panels **(a)** and **(f)** show the contribution of OA species from terpenes (TSOA). Panels **(b)** and **(g)** show the contribution of OA species from isoprene (ISOA). Panels **(c)** and **(h)** show the contribution of OA species from light aromatics & intermediate-volatility organic compounds (ASOA). Panels **(d)** and **(i)** show the contribution of OA species from primary semivolatile organic compounds (POA). Panels **(e)** and **(j)** show the contribution of OA species from oxidized semivolatile organic compounds (OPOA).

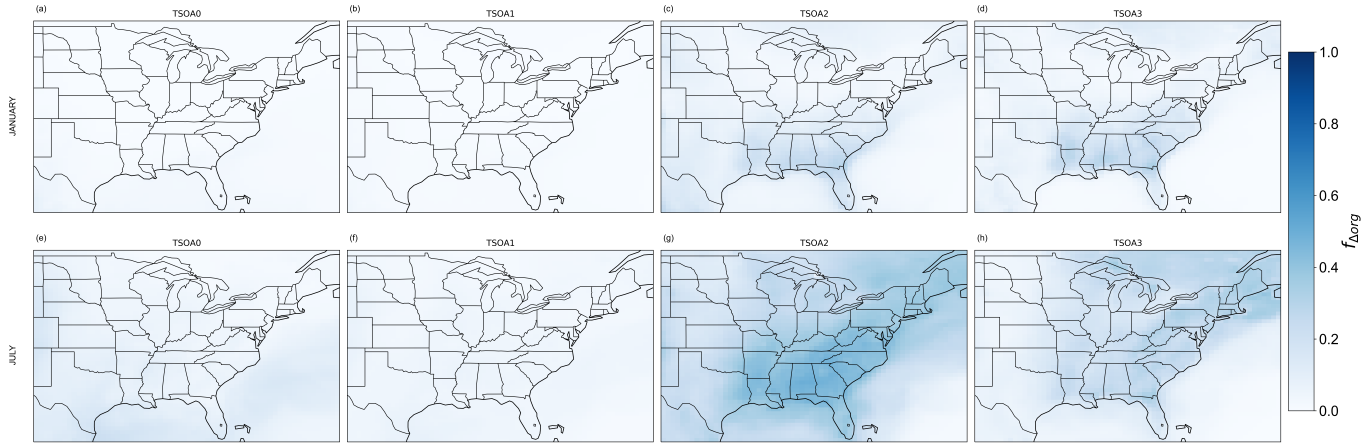

Figure S7. January 2019 (top panels) and July 2019 (bottom panels) monthly mean surface contribution of OA species from terpenes (TSOA) to the absolute difference in OA organic mass concentration, expressed as the organic mass concentration change fraction $f_{\Delta org}$. Panels **(a)** and **(e)** show the contribution of TSOA0 ($C_j^* = 0.1$ µg m^{-3}). Panels **(b)** and **(f)** show the contribution of TSOA1 ($C_j^* = 1$ µg m^{-3}). Panels **(c)** and **(g)** show the contribution of TSOA2 ($C_j^* = 10$ µg m^{-3}). Panels **(d)** and **(h)** show the contribution of TSOA3 ($C_j^* = 100$ µg m^{-3}).

Figure S8. January 2019 (top panels) and July 2019 (bottom panels) monthly mean surface contribution of OA species from isoprene (ISOA) to the absolute difference in OA organic mass concentration, expressed as the organic mass concentration change fraction $f_{\Delta org}$. Panels **(a)** and **(c)** show the contribution of SOAGX ($C_j^* = 0\ \mu g\,m^{-3}$). Panels **(b)** and **(e)** show the contribution of SOAIE ($C_j^* = 0\ \mu g\,m^{-3}$). Panels **(c)** and **(f)** show the contribution of LVOCOA ($C_j^* = 0\ \mu g\,m^{-3}$).

Figure S9. January 2019 (top panels) and July 2019 (bottom panels) monthly mean surface contribution of OA species from light aromatics & intermediate-volatility organic compounds (ASOA) to the absolute difference in OA organic mass concentration, expressed as the organic mass concentration change fraction $f_{\Delta org}$. Panels **(a)** and **(e)** show the contribution of ASOAN ($C_j^* = 0$ µg m^{-3}). Panels **(b)** and **(f)** show the contribution of ASOA1 ($C_j^* = 1$ µg m^{-3}). Panels **(c)** and **(g)** show the contribution of ASOA2 ($C_j^* = 10$ µg m^{-3}). Panels **(d)** and **(h)** show the contribution of ASOA3 ($C_j^* = 100$ µg m^{-3}).

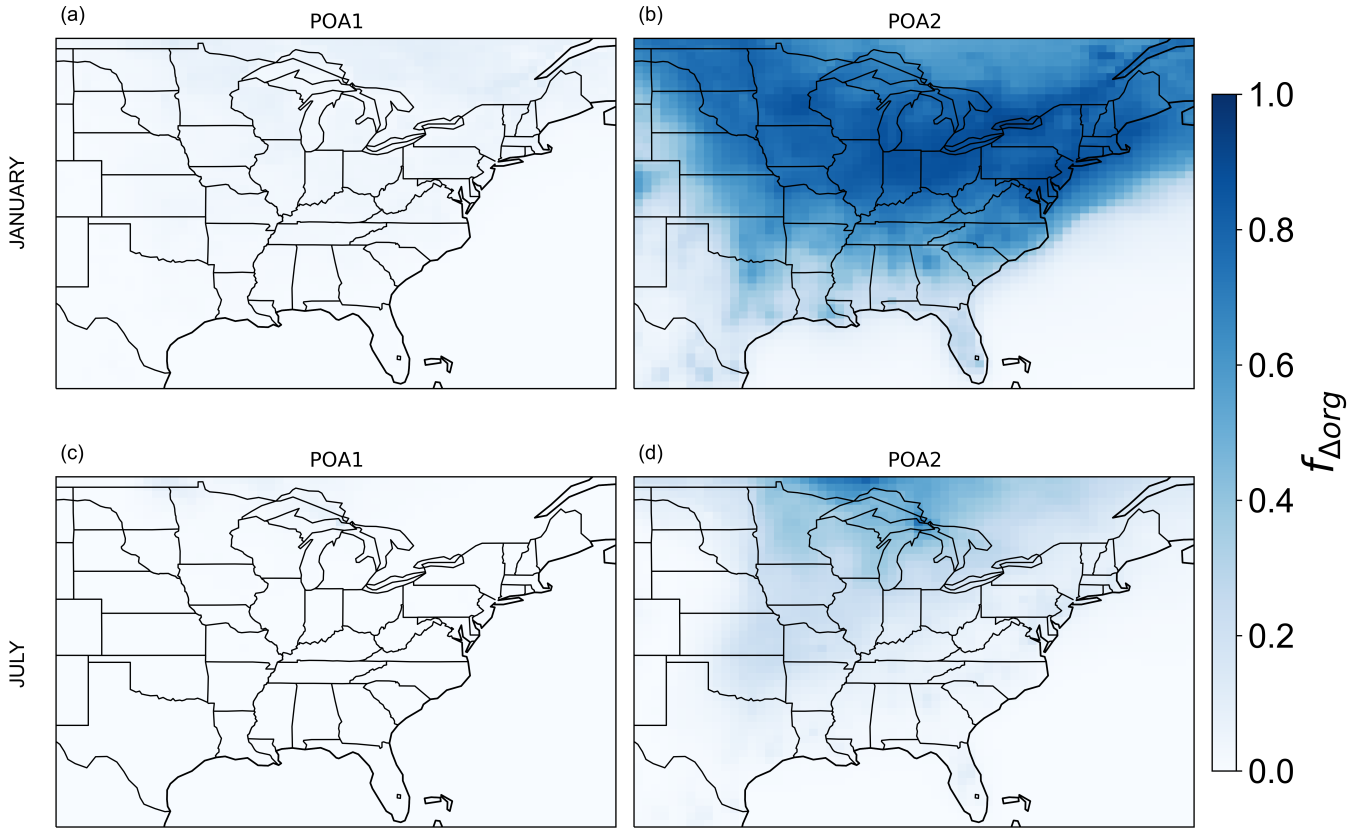

Figure S10. January 2019 (top panels) and July 2019 (bottom panels) monthly mean surface contribution of OA species from primary semivolatile organic compounds (POA) to the absolute difference in OA organic mass concentration, expressed as the organic mass concentration change fraction $f_{\Delta org}$. Panels **(a)** and **(c)** show the contribution of POA1 ($C_j^* = 1646\ \mu g\,m^{-3}$). Panels **(b)** and **(d)** show the contribution of POA2 ($C_j^* = 20\ \mu g\,m^{-3}$).

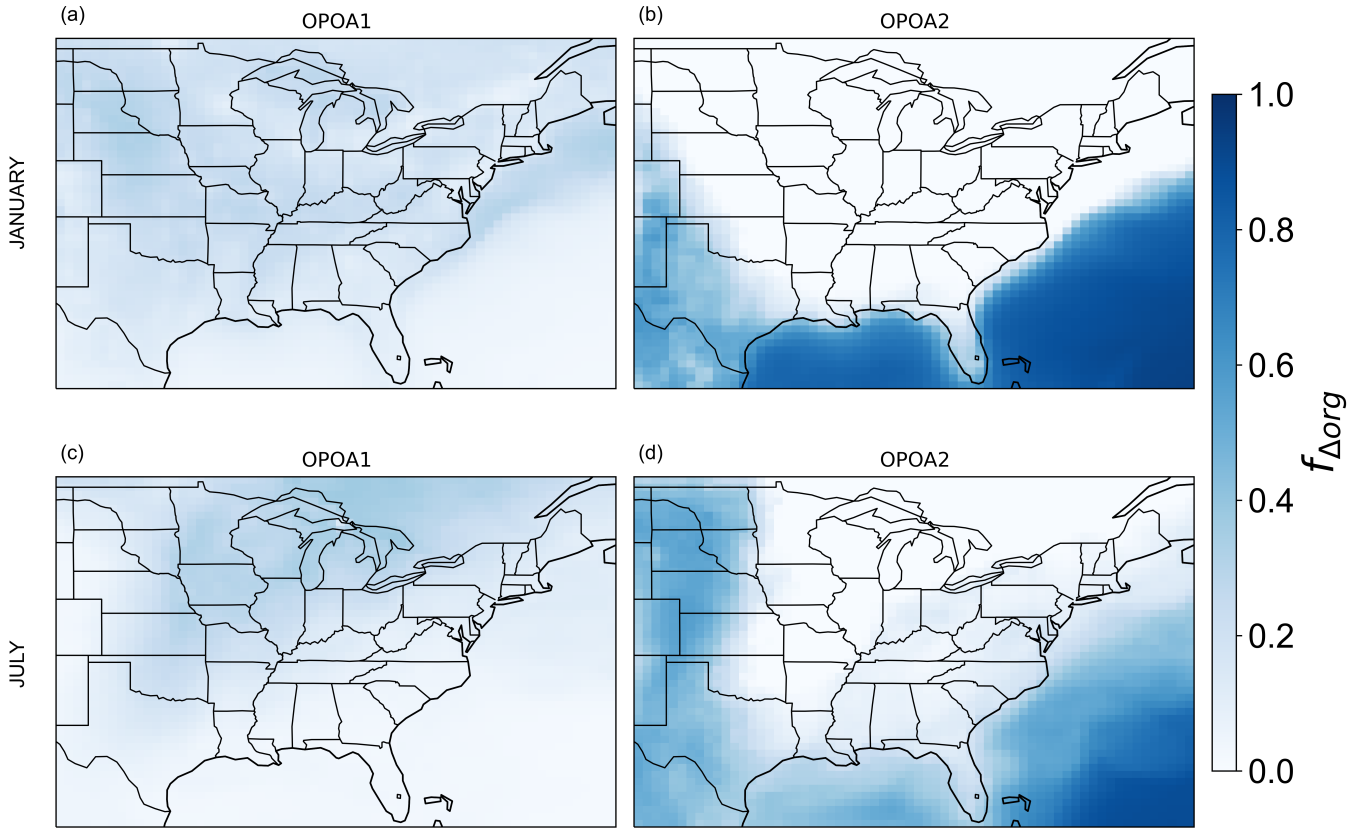

Figure S11. January 2019 (top panels) and July 2019 (bottom panels) monthly mean surface contribution of OA species from oxidized semivolatile organic compounds (OPOA) to the absolute difference in OA organic mass concentration, expressed as the organic mass concentration change fraction $f_{\Delta org}$. Panels **(a)** and **(c)** show the contribution of OPOA1 ($C_j^* = 16.46\ \mu g\,m^{-3}$). Panels **(b)** and **(d)** show the contribution of OPOA2 ($C_j^* = 0.2\ \mu g\,m^{-3}$).

S4 Diurnal Cycle of OA

Figure S12c shows the diurnal cycle of surface OA organic mass concentration for Montreal, Quebec, predicted by the water-sensitive (updated) and the dry (default) OA schemes on July 3–4, 2019. As expected, RH increases from 8 p.m. to 8 a.m. local time the following day, at which point the maximum value is reached. RH then decreases until the cycle restarts in a similar fashion at 8 p.m. The diurnal cycle of atmospheric T follows almost the exact opposite pattern, where T decreases from 8 p.m. to 5 a.m. and reaches its lowest value at 5 a.m. T then increases until the cycle restarts at 8 p.m. The effective volatility of organic compounds typically decreases with decreasing T and increasing RH. The absolute (Fig. S12d) and relative (Fig. S12e) differences in OA organic mass concentrations are calculated using the dry OA scheme as the reference. Positive values mean that the water-sensitive OA scheme predicts a higher OA organic mass concentration than the dry OA scheme. The absolute and relative differences in OA organic mass concentrations closely follow the RH variation over the diurnal cycle: when RH increases (or decreases) with time, so does the difference between the two OA partitioning schemes. The diurnal cycle predicted by the dry OA scheme over Montreal varies due to T fluctuations and organic mass advection effects. Even though both OA schemes are exposed to the same T conditions and OA advection effects, the uptake of water and related feedback on the effective volatility of organic compounds that are accounted for by the water-sensitive scheme enhance the predicted OA organic mass concentration over the dry scheme. In this particular diurnal cycle, the water-sensitive OA organic mass concentration increases by more than 80 $\%$ at 8 a.m. with respect to the dry OA scheme when RH is at its maximum value.

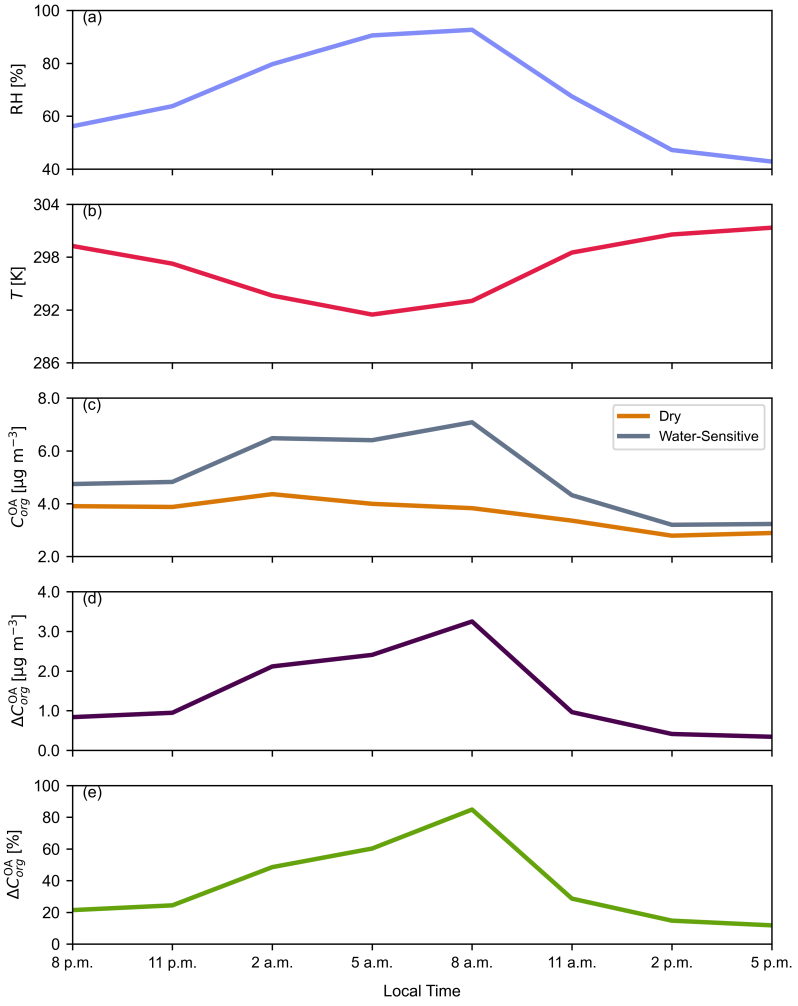

Figure S12. Time series of three-hourly values of surface RH, T, and OA properties predicted by the introduced water-sensitive OA scheme (BAT-VBS model) for Montreal, Canada, on July 3–4, 2019. The panels show: **(a)** the relative humidity, **(b)** the temperature, **(c)** the OA organic mass concentration, **(d)** the absolute difference in OA organic mass concentration, and **(e)** the relative difference in OA organic mass concentration. The absolute and relative differences are calculated using the dry OA scheme of GEOS-Chem as the reference, which in this study corresponds to the water-sensitive OA scheme (BAT-VBS model) at dry conditions ($C_{org,\mathrm{BAT-VBS}}^{\mathrm{OA}}$ (RH) - $C_{org,\mathrm{BAT-VBS}}^{\mathrm{OA}}$ (RH = 0 %)).

S5 Vertical Profile of OA

The hygroscopicity of OA is defined as its water affinity. The ability of OA to capture (and release) moisture from the environment is important for understanding cloud condensation nuclei (CCN) formation in the atmosphere. Petters and Kreidenweis (2007) introduced a relationship between the dry diameter of aerosol constituents and CCN activity. Typically, the hygroscopicity of OA is quantified in large-scale three-dimensional models with a simplified hygroscopicity parameter (κ) (Pankow and Barsanti, 2009; Zhang et al., 2012; Pankow et al., 2015; Jathar et al., 2016; Pye et al., 2017; Kim et al., 2019). This κ parameter relates the water captured by organic compounds in the OA to the composition dependence of the related binary solution water activity, which is equivalent to bulk equilibrium RH (Petters and Kreidenweis, 2007):

$$\frac{1}{a_{water}} = 1 + \kappa_{org}^{\mathrm{OA}} \frac{V_{org}^{\mathrm{OA}}}{V_{water}^{\mathrm{OA}}}, \tag{S6}$$

where a_{water} is the water activity of the aqueous OA solution, $\kappa_{org}^{\mathrm{OA}}$ is the hygroscopicity parameter of the OA, V_{org}^{OA} is the cumulative volume of water-free organic compounds in the OA, and V_{water}^{OA} is the volume of water taken up by organic compounds in the OA at a specified water activity level.

The cumulative volume V_{org}^{OA} can be calculated as the summation of the individual volumes of organic species j in the OA:

$$V_{org}^{\mathrm{OA}} = \sum_{n=1} V_j^{\mathrm{OA}}, \tag{S7}$$

where V_j^{OA} is the water-free volume of the organic compound j.

The cumulative volume V_{water}^{OA} is obtained from the equilibrium OA mass concentration of water due to all the organic species in the OA, which is an output of the BAT-VBS model:

$$V_{water}^{\mathrm{OA}} = \frac{C_{water}^{\mathrm{OA}}}{\rho_{water}^{\mathrm{OA}}}, \tag{S8}$$

where C_{water}^{OA} is the OA mass concentration of water that is taken up by all the organic species j in the OA and $\rho_{water}^{\mathrm{OA}}$ is the density of water.

The cumulative volume V_{org}^{OA} is obtained from the summation of the individual equilibrium OA organic mass concentrations of organic species in the OA, which are also outputs of the BAT-VBS model:

$$V_{org}^{\mathrm{OA}} = \sum_{n=1} \frac{C_j^{\mathrm{OA}}}{\rho_j^{\mathrm{OA}}}, \tag{S9}$$

where C_j^{OA} and ρ_j^{OA} are the OA organic mass concentration and density of the organic species j in the OA, respectively.

The density of the organic species j in the OA can be approximated using its elemental ratios (Kuwata et al., 2012):

$$\rho_j^{\mathrm{OA}} = \frac{12 + (\mathrm{H:C}_j) + 16(\mathrm{O:C}_j)}{7 + 5(\mathrm{H:C}_j) + 4.15(\mathrm{O:C}_j)}, \tag{S10}$$

where $\mathrm{H:C}_j$ and $\mathrm{H:C}_j$ are the hydrogen-to-carbon and oxygen-to-carbon elemental ratios of the organic species j, respectively.

Due to the absence of information about the value of $\mathrm{H:C}_j$ for organic compounds in the OA phase, the elemental ratio was estimated in GEOS-Chem by $\mathrm{H:C}_j \approx 2 - \mathrm{O:C}_j$, using a slope of -1 in a Van Krevelen diagram (H:C vs O:C), which is a common assumption (Heald et al., 2010).

In each grid cell of the GEOS-Chem model, the cumulative organic and water volumes and RH can then be used to estimate the hygroscopicity parameter of the OA according to Eq. (S6).

Figure S14a shows the vertical profile of $\kappa_{org}^{\mathrm{OA}}$ from the first atmospheric level ($0.058\ \mathrm{km}$) up to an elevation of $2\ \mathrm{km}$. The variation of $\kappa_{org}^{\mathrm{OA}}$ with elevation is affected by the composition of OA and RH at each vertical level. Due to its high mass fraction (Fig. S15c) and polarity (Table 2), the oxidized SVOCs species OPOA2 dominates the overall hygroscopicity of the OA within the entire 2 km layer. The vertical profile of the individual mass fractions of organic compounds (f_{org}) in the OA (with respect to the cumulative OA organic mass concentration) is shown in Fig. S15. The vertical profile of f_{org} for the different compound classes in GEOS-Chem is shown in S14b.

The BAT-VBS model does not need to calculate κ to estimate the hygroscopicity of OA and its associated water uptake. This exercise was only done to compare the predictions of the BAT-VBS model with the common assumption adopted in large-scale 3D models to assign a constant κ value to characterize the water affinity of the OA (Pankow and Barsanti, 2009; Zhang et al., 2012; Pankow et al., 2015; Jathar et al., 2016; Pye et al., 2017; Kim et al., 2019). The outputs of the BAT-VBS model can be used to analyze the variation of κ over space and time. The aerosol impact on climate via aerosol–radiation and aerosol–radiation–cloud interactions are sensitive to the parameterized aerosol hygroscopicity and water uptake in large-scale 3D models (Rastak et al., 2017). While not the only source of uncertainty in climate models, using a constant κ to represent the water affinity of OA can lead to considerable errors when estimating the climate impact of aerosols.

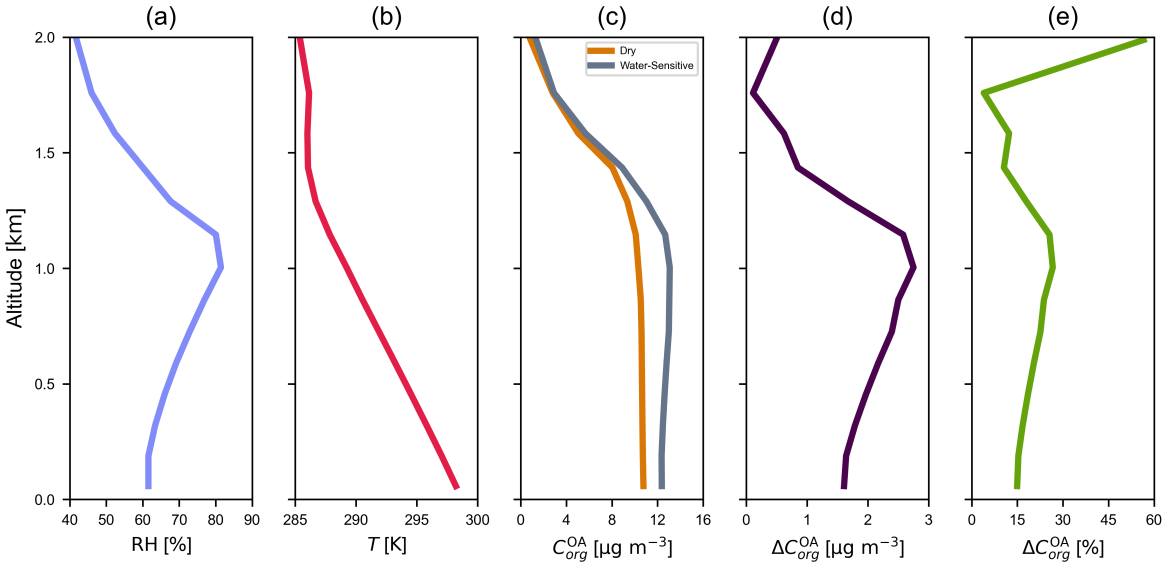

Figure S13. Vertical profile of surface RH, T, and OA properties predicted by the introduced water-sensitive OA scheme (BAT-VBS model) over Montreal, Canada, on July 6, 2019, at 5 p.m. local time. The panels show: **(a)** the relative humidity, **(b)** the temperature, **(c)** the OA organic mass concentration, **(d)** the absolute difference in OA organic mass concentration, and **(e)** the relative difference in OA organic mass concentration. The absolute and relative differences are calculated using the dry OA scheme of GEOS-Chem as the reference, which in this study corresponds to the water-sensitive OA scheme (BAT-VBS model) at dry conditions ($C_{org,\mathrm{BAT-VBS}}^{\mathrm{OA}}$ (RH) - $C_{org,\mathrm{BAT-VBS}}^{\mathrm{OA}}$ (RH = 0 %)).

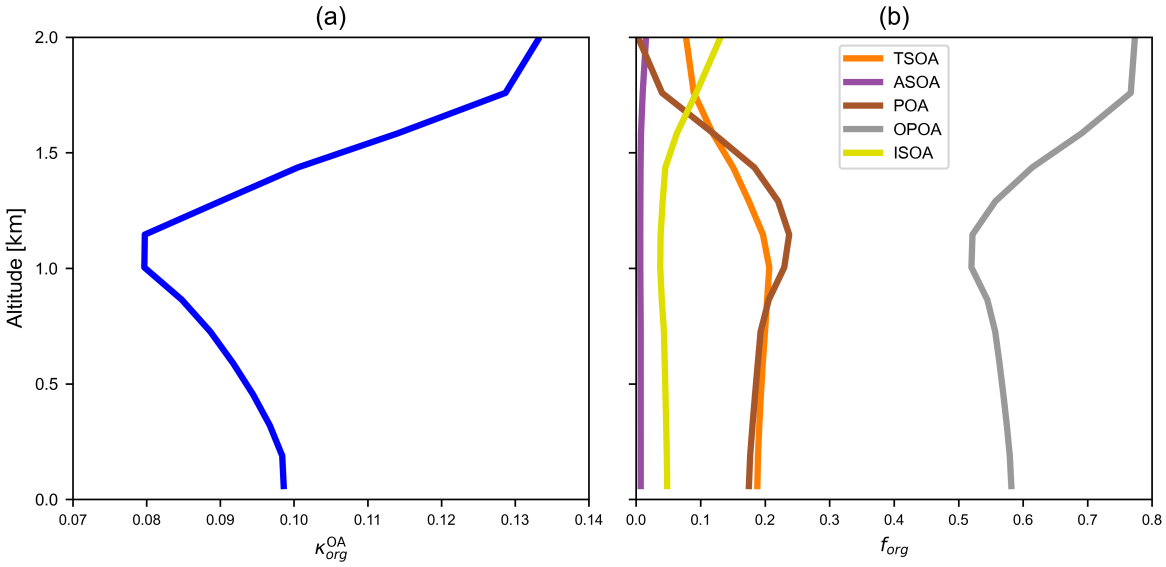

Figure S14. Vertical profile of OA properties predicted by the water-sensitive OA scheme (BAT-VBS model) over Montreal, Canada, on July 6, 2019 (5 p.m. local time). Panel **(a)** shows the OA hygroscopicity parameter. Panel **(b)** shows the contribution of OA compound classes to the OA organic mass concentration, expressed as the organic mass fraction f_{org}.

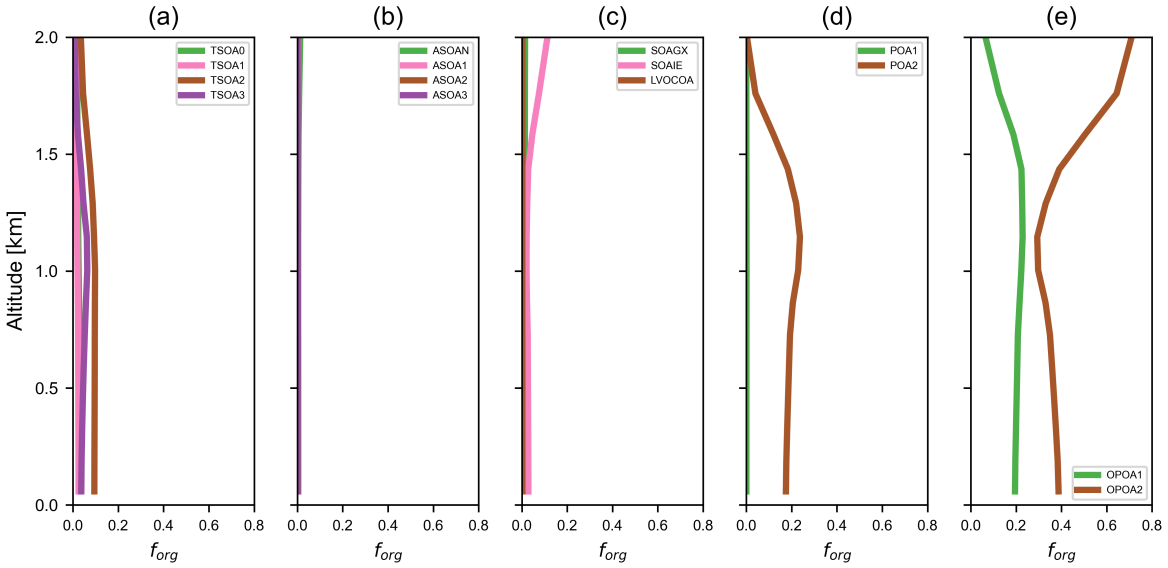

Figure S15. Vertical profile of OA properties predicted by the water-sensitive OA scheme (BAT-VBS model) over Montreal, Canada, on July 6, 2019 (5 p.m. local time). The contribution of OA species to the OA organic mass concentration is expressed as the organic mass fraction f_{org}. Panel **(a)** shows the contribution of OA species from terpenes (TSOA0, TSOA1, TSOA2, and TSOA3). Panel **(b)** shows the contribution of OA species from light aromatics & intermediate-volatility organic compounds (ASOAN, ASOA1, ASOA2, and ASOA3). Panel **(c)** shows the contribution of OA species from isoprene (SOAGX, SOAIE, and LVOCOA). Panel **(d)** shows the contribution of OA species from primary semivolatile organic compounds (POA1 and POA2). Panel **(e)** shows the contribution of OA species from oxidized semivolatile organic compounds (OPOA1 and OPOA2).

S6 RH Threshold for the BAT-VBS model

The water-sensitive (introduced) OA scheme enhances the OA organic mass concentration with respect to the dry (default) OA scheme in any grid cell where RH is above $0\ \%$, as explained in Sec. 3.1.1. In our simulations, described in Sec. 2.1, we used the water-sensitive OA scheme instead of the dry OA schemes in all the grid cells of the GEOS-Chem model. It is possible, however, to reduce the computational costs associated with the introduced OA scheme in GEOS-Chem by limiting the water-sensitive treatment to certain grid cells where RH is above a given threshold and using the dry (default) OA scheme elsewhere. In other words, the water-sensitive OA scheme could be reserved for grid cells where RH conditions lead to a significant enhancement in OA organic mass concentration with respect to the dry OA scheme. The definition of a significant enhancement in OA organic mass concentration is subjective. For example, a GEOS-Chem user might decide that an OA organic mass concentration enhancement of $10\ \%$ or more is considered significant, in which case the BAT-VBS model would be used in all grid cells where RH $> 5\ \%$ and the dry OA schemes elsewhere. Using the outputs of our July 2019 nested simulation, which considers the 72 vertical levels of the North American domain ($-140\ ^\circ$ to $-40\ ^\circ$ longitude and $10\ ^\circ$ to $70\ ^\circ$ latitude), we calculated the mean RH (threshold) value associated with different water-sensitive OA organic mass concentration enhancements ($\Delta C_{org}^{\mathrm{OA}}$) (Tab. S1). In addition, we calculated the frequency of grid cells where RH was greater than the threshold value. For example, $47.4\ \%$ of the grid cells had a RH value greater than $5\ \%$ during July 2019.

Table S1. Water-sensitive OA organic mass concentration enhancement associated with different mean RH conditions over North America

$\Delta C_{org}^{\mathrm{OA}}$ (%)	Mean RH threshold (%)	Frequency of RH values above the RH threshold (%)
10	5.0	47.4
20	9.6	45.3
30	13.5	43.8
40	16.2	42.8
50	18.2	42.1

References

Chung, S. H. and Seinfeld, J. H.: Global distribution and climate forcing of carbonaceous aerosols, Journal of Geophysical Research: Atmospheres, 107, AAC 14–1–AAC 14–33, https://doi.org/https://doi.org/10.1029/2001JD001397, 2002.

Donahue, N. M., Robinson, A. L., Stanier, C. O., and Pandis, S. N.: Coupled Partitioning, Dilution, and Chemical Aging of Semivolatile Organics, Environmental Science & Technology, 40, 2635–2643, https://doi.org/10.1021/es052297c, 2006.

Gorkowski, K., Preston, T. C., and Zuend, A.: Relative-humidity-dependent organic aerosol thermodynamics via an efficient reduced-complexity model, Atmos. Chem. Phys., 19, 13 383–13 407, https://doi.org/10.5194/acp-19-13383-2019, 2019.

Heald, C. L., Kroll, J. H., Jimenez, J. L., Docherty, K. S., DeCarlo, P. F., Aiken, A. C., Chen, Q., Martin, S. T., Farmer, D. K., and Artaxo, P.: A simplified description of the evolution of organic aerosol composition in the atmosphere, Geophysical Research Letters, 37, https://doi.org/https://doi.org/10.1029/2010GL042737, 2010.

Jathar, S. H., Mahmud, A., Barsanti, K. C., Asher, W. E., Pankow, J. F., and Kleeman, M. J.: Water uptake by organic aerosol and its influence on gas/particle partitioning of secondary organic aerosol in the United States, Atmospheric Environment, 129, 142–154, https://doi.org/https://doi.org/10.1016/j.atmosenv.2016.01.001, 2016.

Kim, Y., Sartelet, K., and Couvidat, F.: Modeling the effect of non-ideality, dynamic mass transfer and viscosity on SOA formation in a 3-D air quality model, Atmos. Chem. Phys., 19, 1241–1261, https://doi.org/10.5194/acp-19-1241-2019, aCP, 2019.

Kuwata, M., Zorn, S. R., and Martin, S. T.: Using Elemental Ratios to Predict the Density of Organic Material Composed of Carbon, Hydrogen, and Oxygen, Environ. Sci. Technol., 46, 787–794, https://doi.org/10.1021/es202525q, 2012.

Marais, E. A., Jacob, D. J., Jimenez, J. L., Campuzano-Jost, P., Day, D. A., Hu, W., Krechmer, J., Zhu, L., Kim, P. S., Miller, C. C., Fisher, J. A., Travis, K., Yu, K., Hanisco, T. F., Wolfe, G. M., Arkinson, H. L., Pye, H. O. T., Froyd, K. D., Liao, J., and McNeill, V. F.: Aqueous-phase mechanism for secondary organic aerosol formation from isoprene: application to the southeast United States and co-benefit of SO_2 emission controls, Atmospheric Chemistry and Physics, 16, 1603–1618, https://doi.org/10.5194/acp-16-1603-2016, 2016.

Pankow, J. F.: An absorption model of the gas/aerosol partitioning involved in the formation of secondary organic aerosol, Atmospheric Environment, 28, 189–193, https://doi.org/https://doi.org/10.1016/1352-2310(94)90094-9, 1994.

Pankow, J. F.: Gas/particle partitioning of neutral and ionizing compounds to single and multi-phase aerosol particles. 1. Unified modeling framework, Atmospheric Environment, 37, 3323–3333, https://doi.org/https://doi.org/10.1016/S1352-2310(03)00346-7, 2003.

Pankow, J. F. and Barsanti, K. C.: The carbon number-polarity grid: A means to manage the complexity of the mix of organic compounds when modeling atmospheric organic particulate matter, Atmospheric Environment, 43, 2829–2835, https://doi.org/https://doi.org/10.1016/j.atmosenv.2008.12.050, 2009.

Pankow, J. F., Marks, M. C., Barsanti, K. C., Mahmud, A., Asher, W. E., Li, J., Ying, Q., Jathar, S. H., and Kleeman, M. J.: Molecular view modeling of atmospheric organic particulate matter: Incorporating molecular structure and co-condensation of water, Atmospheric Environment, 122, 400–408, https://doi.org/https://doi.org/10.1016/j.atmosenv.2015.10.001, 2015.

Petters, M. D. and Kreidenweis, S. M.: A single parameter representation of hygroscopic growth and cloud condensation nucleus activity, Atmos. Chem. Phys., 7, 1961–1971, https://doi.org/10.5194/acp-7-1961-2007, 2007.

Pye, H. O. T., Chan, A. W. H., Barkley, M. P., and Seinfeld, J. H.: Global modeling of organic aerosol: the importance of reactive nitrogen (NO_x and NO_3), Atmos. Chem. Phys., 10, 11 261–11 276, https://doi.org/10.5194/acp-10-11261-2010, 2010.

Pye, H. O. T., Murphy, B. N., Xu, L., Ng, N. L., Carlton, A. G., Guo, H., Weber, R., Vasilakos, P., Appel, K. W., Budisulistiorini, S. H., Surratt, J. D., Nenes, A., Hu, W., Jimenez, J. L., Isaacman-VanWertz, G., Misztal, P. K., and Goldstein, A. H.: On the implications of aerosol liquid water and phase separation for organic aerosol mass, Atmos. Chem. Phys., 17, 343–369, https://doi.org/10.5194/acp-17-343-2017, 2017.

Rastak, N., Pajunoja, A., Acosta Navarro, J. C., Ma, J., Song, M., Partridge, D. G., Kirkevåg, A., Leong, Y., Hu, W. W., Taylor, N. F., Lambe, A., Cerully, K., Bougiatioti, A., Liu, P., Krejci, R., Petäjä, T., Percival, C., Davidovits, P., Worsnop, D. R., Ekman, A. M. L., Nenes, A., Martin, S., Jimenez, J. L., Collins, D. R., Topping, D. O., Bertram, A. K., Zuend, A., Virtanen, A., and Riipinen, I.: Microphysical explanation of the RH-dependent water affinity of biogenic organic aerosol and its importance for climate, Geophys Res Lett, 44, 5167–5177, https://doi.org/10.1002/2017gl073056, 2017.

Serrano Damha, C., Cummings, B. E., Schervish, M., Shiraiwa, M., Waring, M. S., and Zuend, A.: Capturing the Relative-Humidity-Sensitive Gas–Particle Partitioning of Organic Aerosols in a 2D Volatility Basis Set, Geophysical Research Letters, 51, e2023GL106 095, https://doi.org/https://doi.org/10.1029/2023GL106095, 2024.

Shiraiwa, M., Berkemeier, T., Schilling-Fahnestock, K. A., Seinfeld, J. H., and Pöschl, U.: Molecular corridors and kinetic regimes in the multiphase chemical evolution of secondary organic aerosol, Atmospheric Chemistry and Physics, 14, 8323–8341, https://doi.org/10.5194/acp-14-8323-2014, 2014.

Zhang, K., O'Donnell, D., Kazil, J., Stier, P., Kinne, S., Lohmann, U., Ferrachat, S., Croft, B., Quaas, J., Wan, H., Rast, S., and Feichter, J.: The global aerosol-climate model ECHAM-HAM, version 2: sensitivity to improvements in process representations, Atmos. Chem. Phys., 12, 8911–8949, https://doi.org/10.5194/acp-12-8911-2012, aCP, 2012.

Zuend, A., Marcolli, C., Luo, B. P., and Peter, T.: A thermodynamic model of mixed organic-inorganic aerosols to predict activity coefficients, Atmos. Chem. Phys., 8, 4559–4593, https://doi.org/10.5194/acp-8-4559-2008, 2008.

Zuend, A., Marcolli, C., Peter, T., and Seinfeld, J. H.: Computation of liquid-liquid equilibria and phase stabilities: implications for RH-dependent gas/particle partitioning of organic-inorganic aerosols, Atmos. Chem. Phys., 10, 7795–7820, https://doi.org/10.5194/acp-10-7795-2010, 2010.

Zuend, A., Marcolli, C., Booth, A. M., Lienhard, D. M., Soonsin, V., Krieger, U. K., Topping, D. O., McFiggans, G., Peter, T., and Seinfeld, J. H.: New and extended parameterization of the thermodynamic model AIOMFAC: calculation of activity coefficients for organic-inorganic mixtures containing carboxyl, hydroxyl, carbonyl, ether, ester, alkenyl, alkyl, and aromatic functional groups, Atmos. Chem. Phys., 11, 9155–9206, https://doi.org/10.5194/acp-11-9155-2011, 2011.